Marilyn N. Raphael · Marika M. Holland

Twentieth century simulation of the southern hemisphere climate in coupled models. Part 1: large scale circulation variability

Abstract The ability of five, global coupled climate models to simulate important atmospheric circulation characteristics in the Southern Hemisphere for the period 1960–1999 is assessed. The circulation features examined are the Southern Hemisphere annular mode (SAM), the semi-annual oscillation (SAO) and the quasi-stationary zonal wave 3 (ZW3). The models assessed are the National Center for Atmospheric Research Community Climate System Model Version 3 (CCSM3), the Commonwealth Scientific and Industrial Research Organisation Mark 3, the Geophysical Fluid Dynamics Laboratory Model, the Goddard Institute for Space Studies Model ER (GISS-ER) and the UK Meteorological Office Hadley Center Coupled Model Version 3. The simulations were compared to the NCAR–NCEP reanalyses. The models simulate a SAO which differs spatially from the observed over the Pacific and Indian oceans. The amplitudes are too high over the southern ocean and too low over the midlatitudes. These differences are attributed to a circumpolar trough which is too deep and extends too far north, and to the inability of the models to simulate the middle to high latitude temperature gradient. The SAM is well-represented spatially by most models but there are important differences which may influence the flow over the Pacific and in the region extending from the Ross to Weddell Seas. The observed trend towards positive polarity in the SAM is apparent in the ensemble averages of the GISS-ER and CCSM3 simulations, suggesting that the trend is due to external forcing by changes in the concentration of ozone and greenhouse gases. ZW3 is well-represented by the models but the observed trend towards positive phases of ZW3 is not apparent in the simulations suggesting that the observed trend may be due to natural variability, not external forcing.

M. N. Raphael (✉)
UCLA Department of Geography, 1255 Bunche Hall,
Los Angeles, CA 90095, USA
E-mail: raphael@geog.ucla.edu
Tel.: +1-310-2064590
Fax: +1-310-206-5976

M. M. Holland
National Center for Atmospheric Research, PO Box 3000,
Boulder, CO 80307, USA
E-mail: mholland@ucar.edu

1 Introduction

In this paper, we examine the ability of five global climate models to simulate important aspects of the large-scale, Southern Hemisphere (SH) climate and variability in the last four decades of the twentieth century. The models are the National Center for Atmospheric Research Community Climate System Model Version 3 (CCSM3), the Goddard Institute for Space Studies Model ER (GISS-ER), the Geophysical Fluid Dynamics Laboratory Model (GFDL-CM2.1) the CSIRO-MK3 Mark 3.0 (CSIRO-Mk3.0) and the United Kingdom Meteorological Office Hadley Center Coupled Model Version 3 (UKMO-HadCM3). These models are chosen because they have an interactive sea-ice component and part of this study focuses upon model simulation of sea-ice and sea-ice atmosphere interactions. Part 1 of this study, focuses on the important modes of large-scale atmospheric circulation variability. The modes of variability of interest are the SH annular mode (SAM), the semi-annual oscillation (SAO) and zonal wave 3 (ZW3). These circulation modes are associated with important features of the high latitude southern climate, such as Antarctic sea-ice (e.g. Liu et al. 2004), and they have undergone changes in the latter part of the twentieth century (e.g. Marshall 2003; Hurrell and van Loon 1994; Raphael 2004). There are indications that some of these changes are forced by external factors including the anthropogenic driven decrease in the Antarctic stratospheric ozone (e.g. Thompson and Solomon 2002).

The models under study here are participating in the Intergovernmental Panel on Climate Change (IPCC) fourth assessment of present and predicted climate. Therefore it is critical that we have some indication of how well they represent the observed climate. This is complicated in that the observations represent a mix of both natural and forced variations. While there is no reason to expect that the natural variations of the real and simulated climate systems will occur at the same time, they should have similar statistical signatures. We examine the mean state and variability simulated by the models and attempt in some cases to suggest why the simulations appear as they do compared to the observed. Part 2 of this study (in this issue) examines the simulated Antarctic sea-ice and the simulated sea-ice atmosphere interactions. This paper has six major divisions. Descriptions of the model simulations and observed data are in Sect. 2, the SAO is discussed in Sect. 3, the SAM is discussed in Sect. 4, ZW3 in Sect. 5 and a Discussion and Conclusions are given in Sect. 6.

The simulations are compared to the NCAR–NCEP reanalysis for the period 1960–1999 (Kalnay et al. 1996). We acknowledge that this dataset has some problems which might influence the comparisons. For example, Hines et al. (2000) showed the presence of anomalous trends in the geopotential height field south of 50S and Marshall (2003) showed that the trends in SLP and the SAM in the reanalysis are over-estimated compared to station data. The spatial representation of the field however is reliable so we do not expect the errors to influence the spatial representation of the modes of atmospheric circulation.

The variables examined are sea level pressure (SLP), surface air temperature, the zonal wind and geopotential heights. Following van Loon (1967) the SAO is calculated using Fourier analysis and the SAM is calculated using principal components analysis, as has been done in numerous preceding studies (e.g. Kidson 1999). The index representing the temporal variation of the SAM is calculated after Gong and Wang (1999).

2 Model simulations and observed data

For simplicity a brief description of the characteristics of the models used in this analysis is given in Table 1. These models are complex and differ in many more ways than are given in Table 1. While these differences might influence the models' results we do not discuss them in this analysis. Instead, references for a detailed analysis of each model are provided in Table 1. One statistically important difference for our analysis is the number of ensemble individuals that make up each model's ensemble mean. This number varies from nine in the case of the GISS-ER to one in the CSIRO-Mk3. Each simulation possesses its own natural variability which will be reduced in an ensemble average. This is useful when the aim of the study is to examine forced signals since, as the number of ensemble members increases, a forced signal if present, is better defined. Much of the discussion below focuses on the model ensemble means. However, we also examine the individual ensemble members thereby allowing comment on both the simulated natural variability and the forced signals. We will discuss differences among the individual ensemble members where they appear important.

3 The semi-annual oscillation

The SAO is an important characteristic of the SH circulation explaining more than 50% of the variability in the SLP. Apparent through the depth of the southern extra-tropical atmosphere, it is manifested by the variation in intensity and position of the Antarctic circumpolar trough (CPT). The CPT contracts, deepens and moves south in March and September and expands, weakens and moves north in June and December. These twice-yearly fluctuations in the CPT are accompanied by similar fluctuations of the tropospheric temperature gradients, geopotential heights, SLP and winds at middle and high latitudes in the SH. The net result is a semi-annual exchange of mass between the Antarctic and midlatitudes so that air moves from north to south twice a year and back (van Loon 1991). While the focus of this research has been on the atmospheric manifestation of the SAO, it has been found in the ocean currents of the extratropics (Large and van Loon 1989) and in the ocean wind stress at the same latitudes (Trenberth et al. 1990).

The SAO is thought to arise from a difference in the cooling and heating rates at latitudes near 50S and 65S

Table 1

	Atmosphere resolution	Ocean resolution	SeaIce resolution	Ensemble size	Reference
CCSM3	1.4×1.4, L26	0.47×1.125, L40	0.47×1.125	7	Collins et al. (submitted)
CSIRO-Mk3.0	1.875×1.875, L18	0.84×1.875, L31	1.875×1.875	1	Gordon et al. 2002
GFDL-CM2.1	2×2.5, L24	1×1	1×1	3	Delworth et al. (submitted)
GISS-ER	4×5, L20	4×5	4×5	8	Schmidt et al. 2005
MIROC3.2(hires)[a]	T106, L56	0.1875×0.28, L47	0.1875×0.28	1	K-1 model developers 2004
UKMO-HadCM3	2.5×3.75, L19	1.25×1.25, L20	1.25×1.25	2	Gordon et al. 2000

[a]This model's results are analyzed in Part 2 (Holland and Raphael 2005, this issue)

where the annual temperature ranges are similar. van Loon (1967) showed that at 50S, cooling in autumn is rapid compared to warming in spring while the reverse is true at 65S. This results in a twice-yearly increase of the temperature gradient (and baroclinicity) between the middle and high latitudes. He related the difference in cooling rates to the heat storage of the upper ocean near 50S. Heat storage in the ocean delays the summer temperature maximum and winter minimum at latitudes near 50S while near (over) Antarctica there is no well-defined winter minimum. Instead temperatures drop rapidly at first in autumn and then decrease more gradually into early spring before rapidly rising into summer. See for example Fig. 3 in Meehl (1991). Using modelling studies, Meehl (1991) provided some evidence to support the idea that ocean heat storage and the annual cycle of sea surface temperature (SST) at 50S were critical to the amplitude and phase of the SAO. Additionally, Simmonds and Walland (1998) suggest that low-frequency variability in the SAO depends on the ocean–atmosphere coupling at middle and high latitudes.

The SAO can vary in amplitude, that is, be weaker than other harmonics in individual years but is always identifiable because its phase is consistent (van Loon and Rogers 1984). The latter is why it dominates the long

term mean in SLP and wind. However, the SAO changed after the late 1970s when the second peak of the harmonic remained strong into November instead of weakening after September. Concurrently, the CPT was deeper in the 1980s than in the decades before. The changes in the SAO have been related to rise in low latitude SSTs, breakdown of the polar stratospheric vortex and a change in the temperature gradient between 50S and 65S. (Hurrell and van Loon 1994; Meehl et al. 1998; Thompson and Solomon 2002). In our evaluation we examine the characteristics of the simulated SAO using the second harmonic of SLP and the zonally-averaged surface air temperature and SLP.

3.1 The second harmonic in SLP

The second harmonic of SLP in the models and observations (Fig. 1) is discussed with respect to its pattern, amplitude and the percentage variance explained. The observed SAO (Fig. 1a) has peak amplitudes (3 hPa) over the oceans near 50S and over Antarctica (5 hPa) and a minimum near 60S. The amplitude minimum occurs at the latitudes where there is a phase reversal from maxima in the transitional seasons (June and December) to the north to maxima in the extreme seasons (March
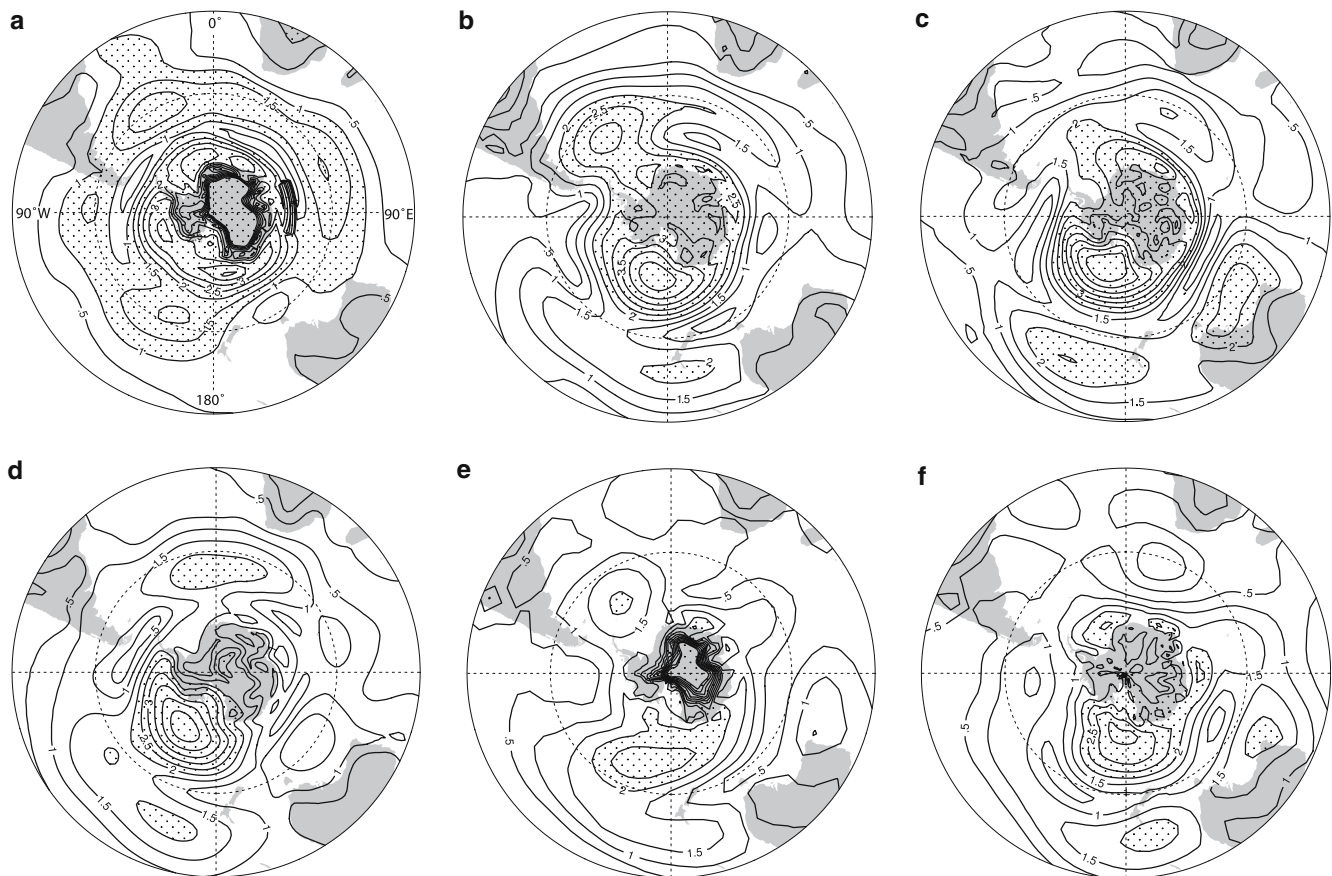
Fig. 1 Second harmonic in sea level pressure (SLP) in the ensemble averages of the **a** NCEP, **b** GFDL-CM2.1, **c** CSIRO-MK3, **d** CCSM, **e** GISS-ER and **f** UKMO-HadCM3 models. Units are hPa. Contour interval is 0.5. *Shaded areas* are above 2 hPa

and September) to the south (Xu et al. 1990). Where the peaks occur, 50% or more of the variance is explained.

All of the models simulate a SAO (Fig. 1b–f) with peak amplitudes near 2 hPa and explaining more than 50% of the variance in regions of peak amplitude (not shown). This is a marked improvement over the models discussed in Xu et al. (1990) where none of the five models analysed could reproduce the general features of the SAO. Although there are these basic similarities between the observed and simulated SAO some important differences are apparent. For example, over the Pacific all of the models simulate a SAO that is too strong, too far north. The CCSM3, CSIRO-Mk3 and UKMO-HadCM3 models place a peak in amplitude, which does not occur in the observed, over and south of Australia. Further, none of the models are able to simulate a true maximum over the Indian ocean, instead, this maximum when it exists is shifted east to lie south of Australia. Only the GISS-ER, GFDL-CM2.1 and CCSM3 models are able to simulate a maximum over the south Atlantic and in the CCSM3 this peak is shifted east of the average observed location. Additionally the amplitude minimum which is found near 60S in the observed is too far north over the Pacific in the simulations particularly in the UKMO-HadCM3. This placement of the amplitude minimum and the lack of an Indian Ocean maximum indicate that the models are unable to capture some important aspects of the spatial variation of the SAO which will ultimately affect the middle and higher latitude climates.

At latitudes higher than 60S the models (except GISS-ER) simulate a SAO that has a higher amplitude than the observed. This fluctuation also extends too far north over the Pacific in concert with the amplitude minimum. The strength of the SAO at these latitudes is associated with a lower than observed SLP and indicates a northern excursion of the CPT (not shown). In each of the models (except the GISS-ER) the CPT, whose outer limits are defined by the 980 hPa isoline, is deeper and extends further north in the months of March and September than observed. The analysis below demonstrates that the simulated CPT is much deeper than observed at 50S and 65S.

3.2 Sea level pressure

The zonally-averaged SLP at 65S and 50S and their difference is shown in Fig. 2. At 50S each model is able to simulate the first peak of the SAO in March. The GISS-ER over-estimates but is still within range of the observed decadal averages (not shown). Interestingly, the second peak in the observed in early southern spring is largely absent from the simulations. The GFDL-CM2.1 simulation exhibits the strongest fluctuation and is a month earlier in phase while the GISS-ER exhibits a very weak second peak in August. The CCSM3, UKMO-HadCM3 and the CSIRO-Mk3 show very weak evidence of a semi-annual fluctuation rather, they have a
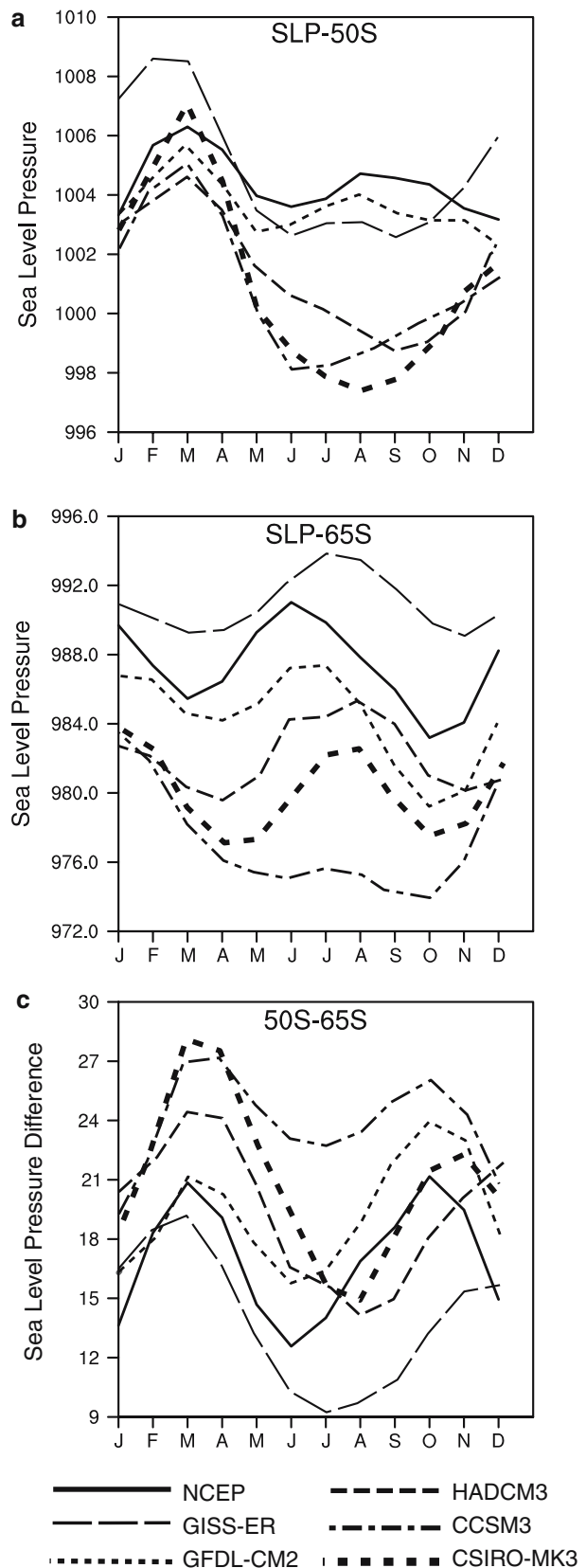
Fig. 2 Zonally averaged SLP at 50S, 65S and their difference for NCEP (*solid black line*), GISS-ER (*thin dashed line*), GFDL-CM2.1 (*thin dotted line*) HADCM3 (*thick dashed line*), CCSM3 (*dash dotted line*) and CSIRO-MK3 (*thick dotted line*). Units are in hPa

very strong annual cycle. In all of the models, spectral analysis of the timeseries of the zonally averaged SLP at 50S (not shown) indicates a very strong annual cycle and a much weaker semi-annual cycle. The UKMO-Had-CM3 spectra has only the annual component. In contrast, the observed timeseries has strong and significant power at 1 year and at 6 months and, most of the power is associated with the 6-month period. These observed spectral characteristics correspond to what is known about SLP in the middle and higher latitudes of the SH, namely, the SAO dominates the variability while the annual signal is weaker by comparison.

At 65S, the average latitude of the CPT, the models are better able to simulate the semi-annual variation. There are important differences in phase between March and October when the observed leads the simulation by at least one month. This means that the observed CPT contracts and deepens faster than the simulated and in the latter the CPT is deeper than observed. Therefore, at 65S over the Pacific, the SAO is out of phase and amplified with respect to the observed. Except for the GISS-ER, all models simulate a deeper than observed CPT, especially the CCSM3. This explains in part the high amplitude of the SAO over the Pacific in the domain of the CPT (Fig. 1).

The difference in SLP (50–65S) (Fig. 2c) shows a very respectable semi-annual variation in all of the models. Given the lack of a second peak at 50S, it appears then that the SAO simulated by the models is driven largely by the fluctuations in SLP at 65S. At 50S the annual cycle is dominant while at 65S, a stronger semi-annual fluctuation is simulated. It is interesting that the models are all able to simulate the annual cycle realistically while failing to reproduce the semi-annual fluctuation. The weakening of the SAO in the 1980s was manifested by a failure of the second peak to occur in September. Instead a reduced peak was observed in November (Meehl et al. 1998) attributed this behaviour of the SAO to a change in the temperature gradient between 50 and 65S such that the gradient peaked in May and November instead of March and September. Therefore we examined the simulated and observed temperature gradients at 500 hPa.

Figure 3 shows the zonally averaged temperature difference at 500 hPa for each model and the observed. This is the index suggested by van Loon (1967) because he found that it was associated with the forcing of the SAO. The observed index (solid black line) experiences the largest temperature gradient in March and October, the smallest in June/July and December/January. Note here that this average contains a decade or more of years when the SAO was reduced and out of phase with the climatological average before 1979. Before 1979, the temperature gradient was largest in September and March. With the exception of GISS-ER, the models do a reasonable job of simulating the large temperature gradient in March. They do not however simulate the second peak in the southern spring very well. The GFDL-CM2.1 closely approximates the observed from June to
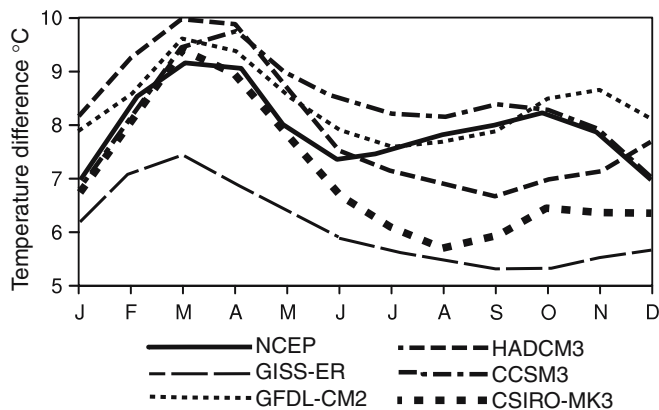
Fig. 3 Zonally averaged temperature difference 50 − 65S for NCEP (*solid black line*), GISS-ER (*thin dashed line*), GFDL-CM2.1 (*thin dotted line*) HADCM3 (*thick dashed line*), CCSM3 (*dash dotted line*) and CSIRO-MK3 (*thick dotted line*). Units are in °K

October but has its second peak in November. This behavior resembles the observed SAO in the period 1979–1994. Meehl et al. (1998) attributed the weakened and phase shifted SAO to changes in the temperature gradient between 50 and 65S. The CSIRO-Mk3 exhibits a weak peak in October, while the CCSM3 has a broad and weak fluctuation stretching from August to October. The GISS-ER and UKMO-HadCM3 do not exhibit a second peak. In general, the simulated 500 hPa temperature gradient in Fig. 3 is consistent with the information gleaned from examining the SLP in Fig. 2. Given the findings of Meehl et al. (1998) and the knowledge that the amplitude of the 500 hPa temperature gradient is important to the intensification and poleward movement of the CPT (van Loon 1967), Fig. 3 suggests that the weak SAO produced by the models is linked to their inability to simulate the temperature gradient between 50 and 65S. Given also the lack of a second peak in the zonally averaged SLP at 50S, we suggest that the reason for this inability in the models may lie in their simulation of the temperature cycle at 50S.

4 The Southern Hemisphere annular mode

The SAM is the leading mode of low frequency variability in the SH troposphere. It describes the month-to-month variability in the zonally varying geopotential height in the troposphere. It is characterised by a largely zonally symmetric structure and emerges as the leading empirical orthogonal function of zonally varying geopotential height. Like the SAO, the SAM involves exchanges of mass between middle and high latitudes. It occurs in the troposphere year-round and in the stratosphere in late southern winter/early spring. Its change of phase occurs generally near 45S (but near 60S, over the Drake Passage) with centers of action over the midlatitude oceans and near 57S over the Pacific. The SAM has shown a trend toward decreased atmospheric pressure over the Antarctic, termed positive polarity, and

increased atmospheric pressure over midlatitudes in the last 3 decades of the twentieth century (Marshall 2003; Thompson and Wallace 2000). The result of such a trend would be an intensification of the polar vortex and faster circumpolar westerly flow (Hurrell and van Loon 1994; Meehl et al. 1998; Thompson and Wallace 2000). The trend in the SAM has been associated with cold anomalies over Antarctica except over the Peninsula where enhanced westerlies advect warm oceanic air onto the land. It has been suggested that the latter is a contributory reason for the enhanced breakup of ice seen in that sector. Thompson and Solomon (2002) suggest that this trend is consistent with changes in stratospheric ozone levels. Kiehl et al. (1988) showed that the response of the stratosphere to decreased levels of ozone is to intensify and delay breakdown of the polar vortex.

4.1 The EOF—spatial pattern

In this study the SAM is represented by the leading EOF of the 850 hPa geopotential height field. The SAM is characterized by its shape (largely zonally symmetric), amplitude, amount of variance explained and the latitude at which it changes phase. Its observed major spatial features (Fig. 4a) are the wave 3 pattern over the midlatitude oceans, the location of the change of phase and the prominent center of action, over the high latitude Pacific region. Each model resolves a very clear SAM (Fig. 4b–f) with a percentage variance explained from 19.41–24.5%, arguably within the range expected from observations. However, comparison with the observed (Fig. 4a) reveals significant differences in shape, orientation and amplitude. Note that Fig. 4b–f is derived from a concatenation of the data not an ensemble average, so the amplitude is not reduced but is a faithful representation of all the characteristics of the simulations. The CCSM3 (Fig. 4d) simulates the weakest amplitude SAM, half that of the observed, (measured by the difference between the centers of action over Antarctica and 45S) while the GISS-ER (Fig. 4e) simulates one almost twice as large. The other models simulate amplitudes that are comparable to that observed.

The midlatitude, oceanic, wave 3 pattern is simulated only by the CCSM3, GFDL-CM2.1 (Fig. 4b), GISS-ER and CSIRO-Mk3 (Fig. 4c) models. In terms of amplitude and orientation, the center of action over the Pacific is simulated by all the models but its placement is best in the CSIRO-Mk3 and GFDL.CM2.1. The GISS-ER and GFDL-CM2.1 models simulate a SAM which is more zonally symmetric than observed in the eastern Hemisphere. The orientation of the SAM in the CCSM3 is
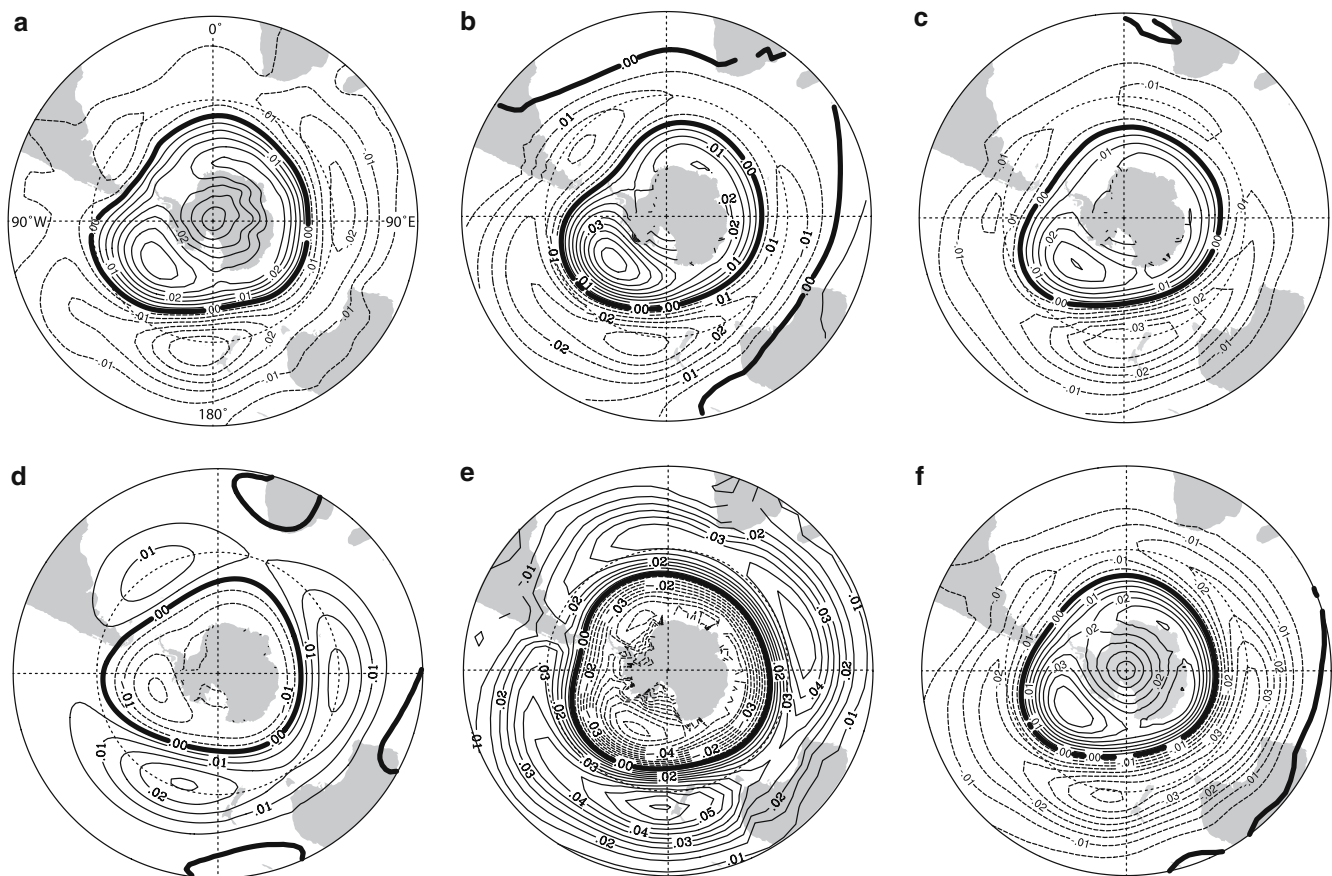
Fig. 4 Leading empirical orthogonal function in the geopotential height field at 850 hPa in **a** NCEP **b** GFDL-CM2.1, **c** CSIRO-MK3, **d** CCSM3, **e** GISS-ER and **f** UKMO-HadCM3

very strongly east/west because the center of action is aligned strongly along the 90W meridian, influencing the south east Pacific rather than the central. However, three of the seven of the individual runs that make up the CCSM3 ensemble mean simulate a SAM that more closely resembles the orientation of the observed. The other four realizations exhibit a SAM that is very like that in Fig. 4c. Additionally, decadal analysis of the observed SAM (not shown) indicates that the average spatial pattern (Fig. 4a) exists in most decades but that in 1970–1979 the orientation of the EOF describing the SAM strongly resembles that shown in Fig. 4c. This indicates that there is temporal variability in the orientation of the observed spatial pattern and that the SAM simulated by the CCSM3 belongs in the range of what can occur in the observed climate system.

The shape and orientation of the Pacific "arm" of the SAM indicates the pattern of flow in that region. The flow is cyclonic and thus influences the local heat flux into the Bellingshausen/Amundsen Seas and out of the Ross Sea. There are also potential influences on the sea-ice distribution via temperature advection and mechanical advection of sea-ice. This circulation pattern allows the advection of warmer oceanic air into the Bellings-hausen/Amundsen Seas and onto the Antarctic Peninsula. It also encourages the flow of cooler air off the continent and the flow of ice out of the Ross Sea perhaps leading to more sea-ice formation as ocean surfaces are exposed (e.g. Lefebvre and Goosse 2005). The SAM simulated by the CCSM3, GFDL-CM2.1, CSIRO-Mk3 and the UKMO-HadCM3 appear best able to allow this sort of flow/ice interaction. A fuller discussion of the influence of the simulated SAM on sea-ice occurs in Part 2 of this study (Holland and Raphael 2005; this issue).

The change of phase of the SAM, i.e. the zero contour on Fig. 4, marks the separation between the colder Antarctic air and the warmer midlatitude air. This is particularly important in the west Antarctic/South American region where because of the shape of the land masses, relatively small latitudinal shifts of the change of phase would determine whether the Antarctic peninsula, for example, is influenced by warmer or colder air. Except for the CSIRO-Mk3 and the GFDL-CM2.1, all of the models simulate a change of phase which extends too far north over South America and could have consequences for their representation of the average temperature over southern South America and for the influence of the SAM on surface features such as sea-ice in the region extending from the Ross to Weddell Seas.

4.2 The SAM index

An often-used index of the SAM is the timeseries of the leading EOF. However, Gong and Wang (1999) have defined a robust index of the SAM using the difference in SLP at 40 and 60S. We use that index here on the model ensemble means where available, and on the individual simulations. Figure 5 shows the timeseries of the SAM index produced by each model and the observed. Their spectra is shown in Fig. 6. Each model simulates a SAM index that has similar timescales of variability as the observed—approximately 4 and 3 months. Interestingly, the GISS-ER, and CCSM3 (the models with the largest ensemble set) also simulate statistically significant, with respect to the red noise spectrum, low-frequency variability (near 16 years) as does the observed. This significant low-frequency appears only in two of the GISS-ER ensemble members. Five show strong but not significant power at 16 years and the other two show very little variability at 16 years. A similar situation exists for the CCSM3 model where, at 16 years, only one run has significant power, four show strong but not significant power, and two runs exhibit little or no significant variability. It seems then that the ensemble averaging has reduced the natural variability in the simulations of both the GISS-ER and CCSM3 models thereby allowing a forced signal to dominate the spectra of the ensemble means.

This low-frequency variability represents the apparent trend to positive values of the SAM index seen in the timeseries of the ensemble means of these models (Fig. 5c, d) and in the observed data beginning from about the mid 1970s (Fig. 5a). Marshall (2003) shows that this positive trend is over-estimated in the Reanalysis but is significant in station data. Several studies (e.g. Fyfe et al. 1999; Cai et al. 2003) suggest that positive trends such as those exhibited by the GISS-ER, and CCSM3 models are due to ozone depletion which along with observed changes in greenhouse gases, volcanic forcing and solar irradiance is one of the few elements that these models may have in common. We suggest then that the trend simulated by these models is linked to the stratospheric ozone changes applied in the models and is not an expression of their natural variability.

Because of the complexity of these models we cannot say with certainty why the CSIRO-Mk3, UKMO-Had-CM3 and GFDL-CM2.1 models do not simulate this trend but it is notable that in the current analysis they have very few ensemble members compared to the CCSM3 and GISS-ER. (See Table 1.) We note as well that the GFDL-CM2.1 ensemble mean spectra has large but not significant power near 16 years. Among its individual members, at 16 years, one has strong but not significant power, another shows weak power and the third has none. The fact that there is such a large range in the spectra simulated by this model suggests that its natural variability is very large compared to the forced response. Therefore when there are few ensemble members the natural variability can overwhelm the forced signal represented by the trend. This suggests that the natural variability in the models examined here may be too large compared to the forced response since the observations exhibit this clear, statistically significant trend toward positive polarity with only one realization which includes both the natural and forced variations of the real world. However, more work is need to assess this issue quantitatively.
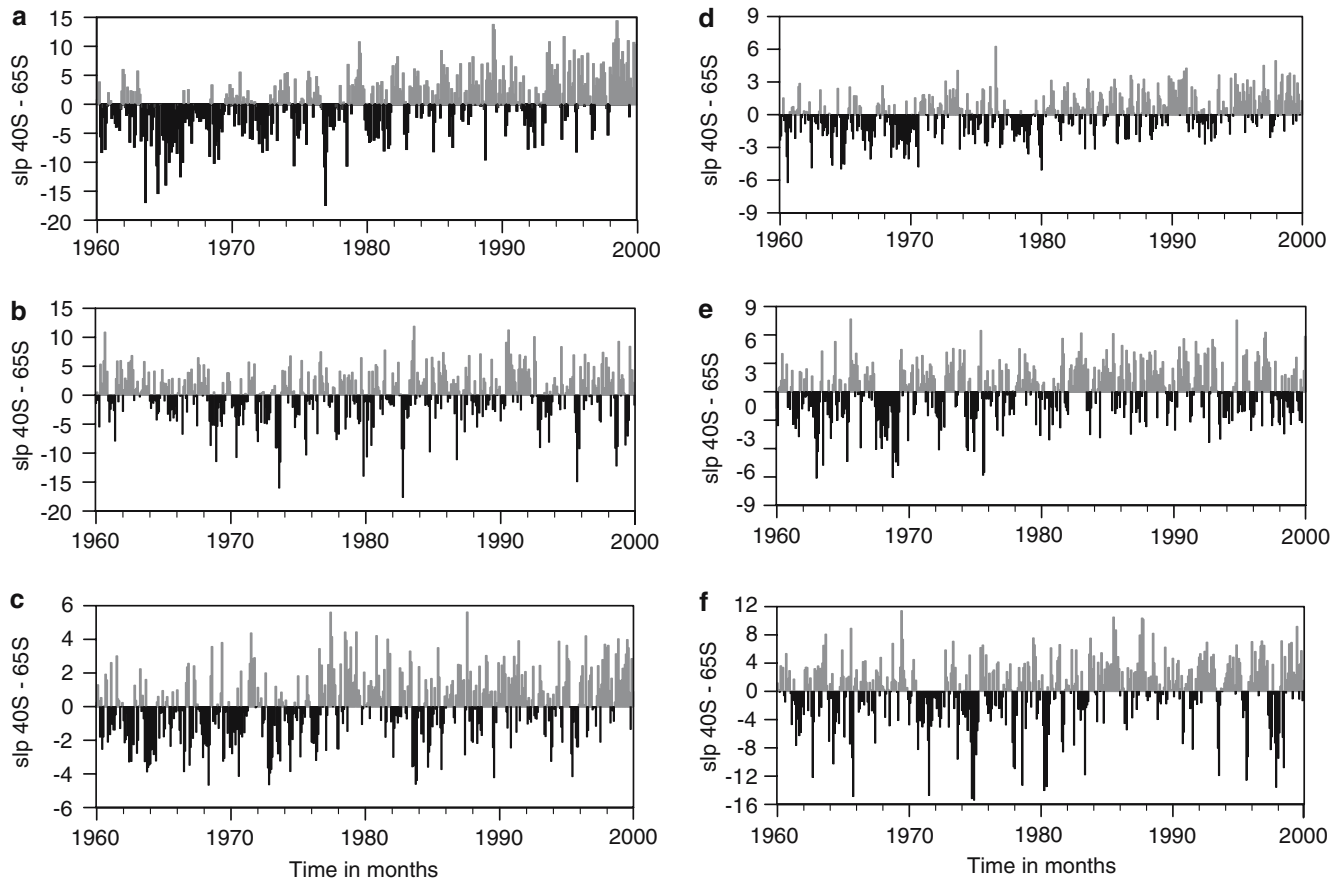
Fig. 5 Timeseries of the index of the Southern Hemisphere annual mode (SAM), **a** NCEP, **b** CSIRO-Mk3, **c** GISS-ER, **d** CCSM3, **e** GFDL-CM2.1, **f** UKMO-HadCM3

The trend toward a positive SAM index is marked by, among other things, an intensification of the observed polar vortex. To determine if this was also true in the models we created composite differences of the zonal wind at 200 hPa based on the extreme positive and negative SAM indices for NCEP and for the GISS-ER and CCSM3 models (Fig. 7). Like the observed (Fig. 7a) both models exhibit an increase in zonal windspeed in the positive phase SAM but it is much better organized in the CCSM3 (Fig. 7b) than in the GISS-ER (Fig. 7c). Additionally, the increase in the zonal wind is much larger in the CCSM3 (4 ms^{-1}) than in the GISS-ER (1 ms^{-1}) but both are smaller than observed (10 ms^{-1}).

5 Zonal wave 3

Zonal wave 3 is the asymmetric part of the large-scale atmospheric circulation associated with meridional flow in the extra-tropical SH. It is quasi-stationary and it contributes to 8% of the spatial variance in the field reaching a maximum near 50°S. Its ridges generally lie downstream of the southern continents (van Loon and Jenne 1972). ZW3 is a dominant feature of the circulation on daily (e.g. Kidson 1988), seasonal (e.g. Mo and

White 1985) and interannual (e.g. Karoly 1989) time-scales at latitudes 45–55°S. Trenberth (1980) shows that it contributes significantly to monthly and interannual circulation variability and it has been associated with blocking in the SH (e.g. Trenberth and Mo 1985). Raphael (2004) created an index of ZW3 in order to facilitate examination of its temporal variability. That study showed that ZW3 has identifiable positive and negative phases associated with the meridionality of the flow and that beginning in the late 1970s ZW3 strengthened and the large-scale flow became more meridional. This state continued for the rest of the century with the exception of the years 1995–1996. Because it reflects the meridional component of the large-scale circulation and therefore the north/south transport of warmer/colder air ZW3 can have an influence on sea-ice concentration which is one of the reasons it is examined here. We use that index here to characterize the simulated ZW3.

5.1 ZW3: spatial pattern and temporal variability

To examine how well the models simulate ZW3, we calculated the 500 hPa fields for the positive and negative phases of ZW3 and their composite differences for
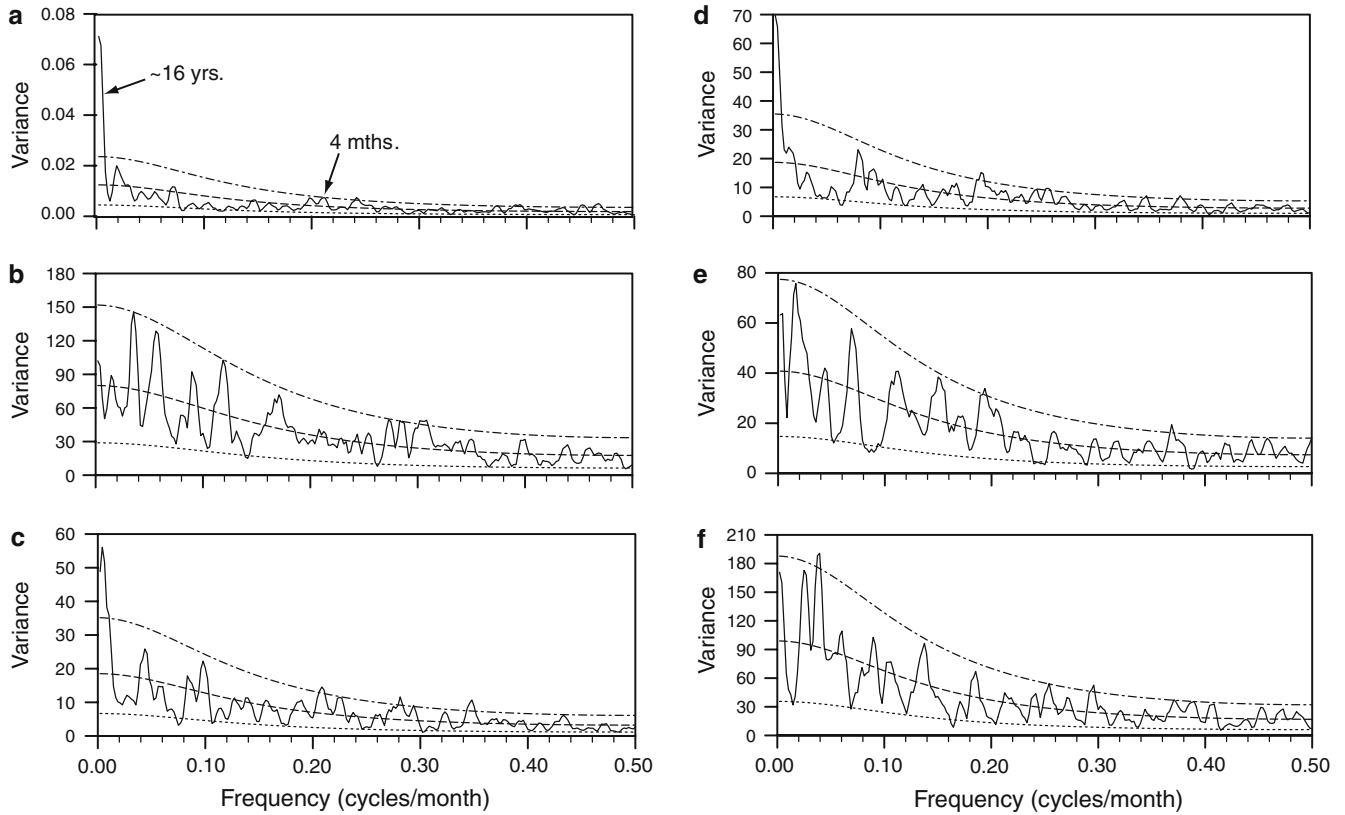
Fig. 6 Spectra of the index of the SAM **a** NCEP, **b** CSIRO-Mk3, **c** GISS-ER, **d** CCSM3, **e** GFDL-CM2.1, **f** UKMO-HadCM3

each model. As for the SAO and SAM, we used the concatenated data in these calculations. Shown in Fig. 8 are the simulated and observed composite differences. It seems clear that the models do a respectable job of simulating ZW3 spatially. The placement of the ridges and troughs that describe ZW3 and their relative amplitudes hews very closely to that observed. The fidelity of the simulated ZW3 to the observed suggests that the associated fluxes of energy and the Antarctic sea ice interactions with ZW3 will be well-represented in the models.

The timeseries of the ZW3 index for each model and the observed are shown in Fig. 9. Substantial variability at low and high frequencies are clear although none of the models show the clear shift to the positive phase that is apparent in the observed (Fig. 9a). Spectrally, the timeseries of the index (not shown) are similar to each other and to the observed and rather white. The observed ZW3 has significant variability at 8 years, 8 and 4 months. The low frequency variability (8 years) is an expression of the trend towards the positive phase of the index noted in Fig. 9a and by Raphael (2004). All of the
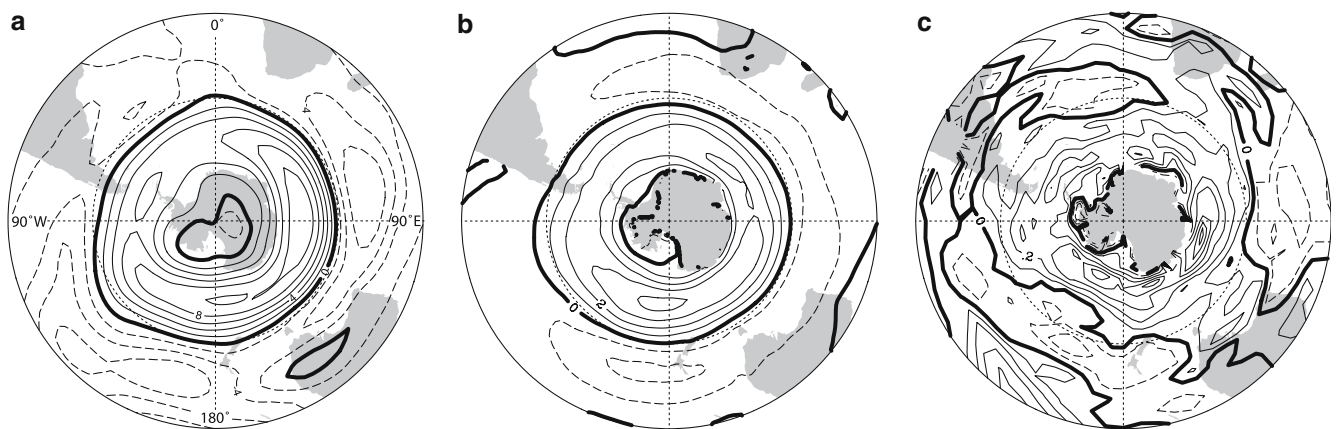
Fig. 7 Composite zonal wind differences of positive phase minus negative phase of the SAM index. **a** NCEP, **b** CCSM3, and **c** GISS-ER. Units are in m/s
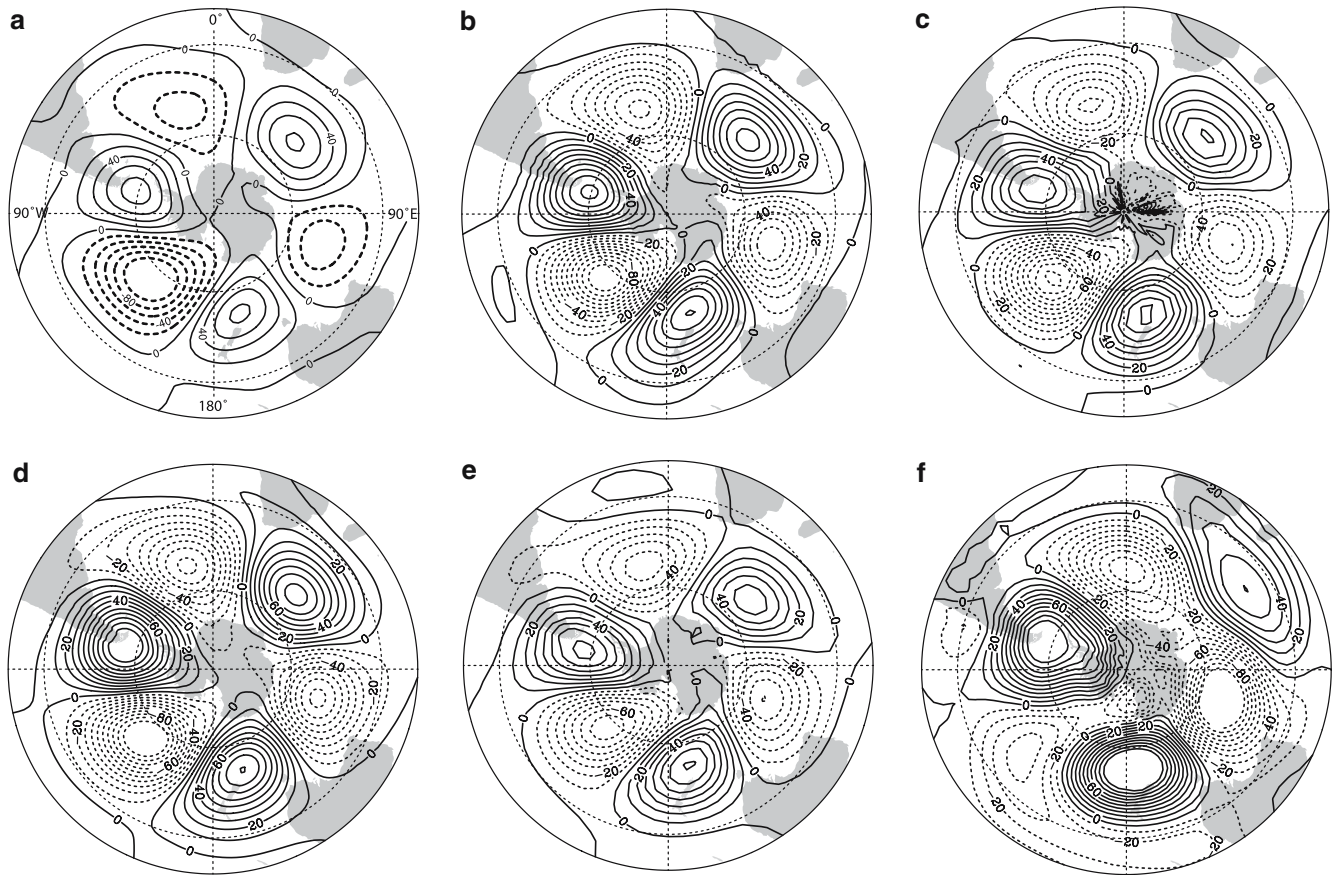
Fig. 8 Zonal wave 3 (ZW3), positive minus negative phase, in the geopotential height field at 500 hPa. **a** NCEP, **b** GFDL-CM2.1, **c** CSIRO-Mk3, **d** CCSM3, **e** GISS-ER, **f** UKMO-HadCM3. Units are in hPa
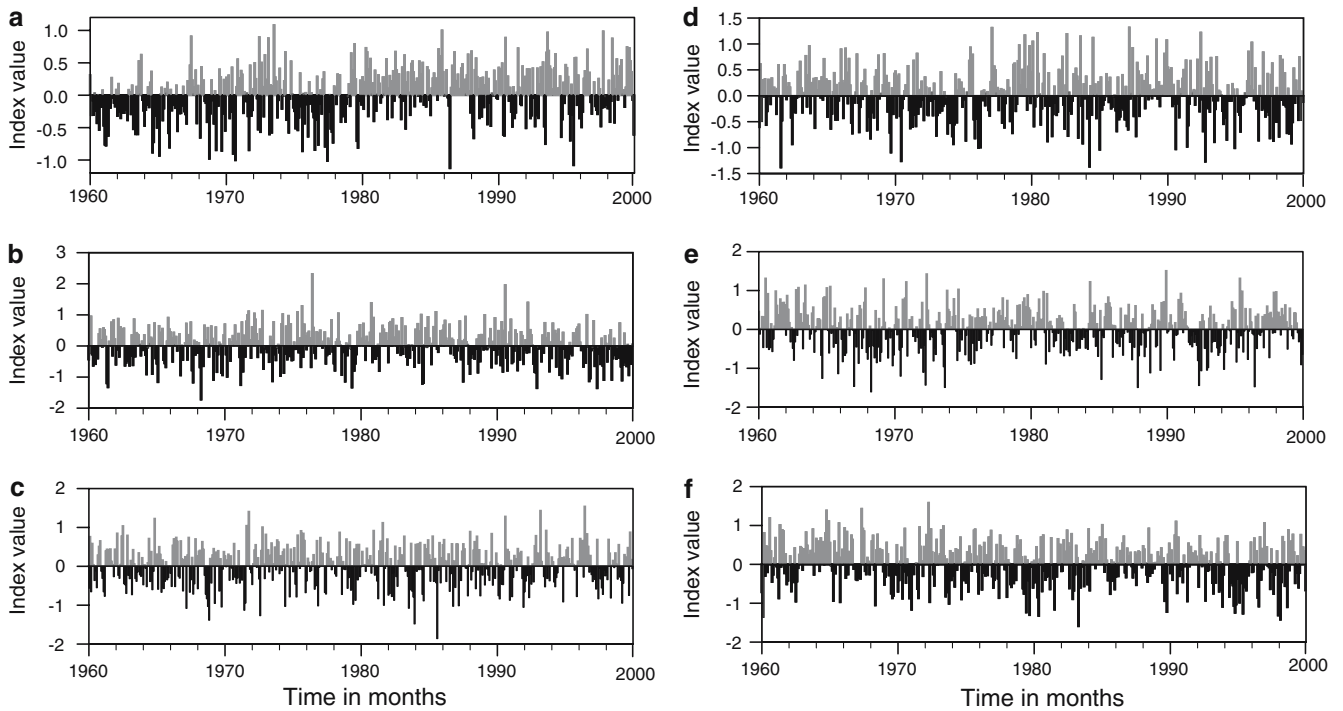
Fig. 9 Timeseries of ZW3 index at 500 hPa. **a** NCEP, **b** CCSM3, **c** GFDL-CM2.1, **d** GISS-ER, **e** CSIRO-Mk3, **f** UKMO-HadCM3

models are able to simulate the higher frequency variability with varying degrees of success. This suggests that they may be used for examining the changes in high frequency variability in the twenty-first century. Only the GISS-ER, CSIRO-Mk3 and UKMO-HadCM3 models are able to simulate the significant peak in variability at 8 years. The low-frequency variability does not appear in the ensemble averages of the GFDL-CM2.1 and CCSM3 models although it is seen in some of the individual members. This suggests that the shift to positive phase seen in the observed in the mid 1970s may be due to natural rather than forced variability.

6 Summary and conclusions

In this study we evaluated the ability of five fully-coupled climate models to reproduce the mean state and variability of the SAO, the SAM and quasi-stationary ZW3. These models are all participants in the fourth assessment of the Intergovernmental Panel on Climate Change (IPCC-AR4) therefore it is necessary that we know how well they simulate important features of the atmospheric circulation and climate.

Model representation of the SAO shows a marked improvement over the models of the 1990s. Some of the spatial characteristics of the SAO are captured but the models simulate higher than observed amplitudes in the sub-Antarctic and lower than observed over the midlatitude oceans. The higher amplitudes in the sub-Antarctic are associated with a too strong CPT and the low amplitudes at midlatitudes appear related to inadequate simulation of the 500 hPa temperature gradient between 50S and 65S. The inability of these models to simulate the temperature gradient at 50–65S limits their use in predictive studies of long term SAO variation. This gradient is important to the intensification and movement of the CPT, a definitive feature of the SAO.

Each model simulates a clear SAM but the shape and orientation of the spatial patterns vary. The GISS-ER model simulates a SAM that is much too concentric, compared to the observed and to the other models. The CCSM3 on the other hand simulated a SAM that is strongly oriented towards the eastern Pacific while on average, the observed SAM is oriented to the central Pacific. The shape of the SAM is an indication of the direction of flow and this is especially important in the sector extending from the Ross to Weddell Seas. The models simulate this with varying levels of success, a factor that must be taken into consideration especially if changes in ice-atmosphere interaction is the study aim.

The trend towards positive polarity in the SAM, observed since the mid 1970s, appears clearly in the ensemble averages of the CCSM3 and GISS models. The associated increase in zonal wind strength at high latitudes and weaker winds at midlatitudes are also apparent and best represented in the CCSM3. The appearance of this trend in these models support the argument that the trend is externally forced by reduced stratospheric ozone concentrations applied in the models and observed over the last decades of the twentieth century. In the current study, the GFDL-CM2.1 model shows strong but not significant variability at low frequency and the lack of significance here may be due to the small number of ensemble members. We suggest that the natural variability in the models examined here may be too large compared to the forced response since the forced response is clear only when the number of ensemble members is large.

The models do a respectable job of simulating ZW3 with respect to both its spatial pattern and its temporal variability. However, the trend towards positive phases of ZW3 noted in the observed does not appear in the ensemble averages of the models suggesting that the observed trend may be due to natural rather than forced variability.

References

Cai W, Whetton PH, Karoly DJ (2003) The response of the Antarctic Oscillation to increasing and stabilized atmospheric CO2. J Clim 16:1525–1538

Fyfe JC, Boer GJ, Flato GM (1999) The Arctic and Antarctic oscillations and their projected changes under global warming. Geophys Res Lett 26:1601–1604

Gong D, Wang S (1999) Definition of the Antarctic oscillation index. Geophys Res Lett 26:459–462

Gordon HB, Rotstayn LD, McGregor MR, Dix MR, Kowalczyk EA, O'Farrell SP, Waterman LJ, Hirst AC, Wilson SG, Collier MA, Watterson IG, Elliot TI (2002) The CSIRO Mk3 Climate System Model. CSIRO Atmospheric Research Technical Paper no. 60, 134 pp

Gordon C, Cooper C, Senior CA, Banks H, Gregory JM, Johns TC, Mitchell JFB, Wood RA (2000) The simulation of SST, sea ice extents and ocean heat transports in a version of the Hadley Centre coupled model without flux adjustments. Clim Dyn 16:147–168

Hines KM, Bromwich DM, Marshall GJ (2000) Artificial surface pressure trends in the NCAR–NCEP reanalysis over the Southern Ocean and Antarctica. J Clim 13:3940–3952

Holland MM, Raphael MN (2005) Twentieth century simulation of the Southern Hemisphere climate in coupled models. Part II: sea ice conditions and variability (this issue)

Hurrell JW, van Loon H (1994) A modulation of the atmospheric annual cycle in the Southern Hemisphere. Tellus 46A:325–338

K-1 model developers (2004) K-1 coupled model (MIROC) description, K-1 technical report, 1. In: Hasumi H, Emori S (eds) Center for Climate System Research, University of Tokyo, p 34

Kalnay E et al (1996) The NCEP/NCAR 40-Year Reanalysis project. Bull Am Met Soc 77:437–472

Karoly DJ (1989) Southern Hemisphere circulation features associated with El Nino-Southern oscillation events. J Clim 2:1239–1251

Kidson JW (1988) Interannual variations in the Southern Hemisphere circulation. J Clim 1:1177–1198

Kidson JW (1999) Principal modes of Southern Hemisphere low-frequency variability obtained from NCEP/NCAR reanalyses. J Clim 12:2808–2830

Kiehl JT, Boville BA, Briegleb BP (1988) Response of a general circulation model to a prescribed Antarctic ozone hole. Nature 332:501–504

Large WG, van Loon H (1989) Large scale, low frequency variability of the 1979 FGGE surface buoy drifts and winds over the Southern Hemisphere. J Phys Oceanogr 19:216–232

Lefebvre W, Goosse H (2005) Influence of the Southern Annular Mode on the sea ice-ocean system: the role of the thermal and mechanical forcing. Ocean Science Discuss 2:299–329

Liu J, Curry JA, Martinson DG (2004) Interpretation of recent Antarctic sea ice variability. Geophys Res Lett 31 doi:10.1029/2003GL018732

van Loon H (1967) The half-yearly oscillations in middle and high Southern latitudes and the coreless winter. J Atmos Sci 24:472–486

van Loon H, Rogers JC (1984) Interannual variations in the half-yearly cycle of pressure gradients and zonal winds at sea level on the Southern Hemisphere. Tellus 36A:76–96

Marshall GJ (2003) Trends in the Southern annular mode from observations and reanalyses. J Clim 16:4134–4143

Meehl GA (1991) A re-examination of the mechanism of the semi-annual oscillation in the Southern Hemisphere. J Clim 4:911–926

Meehl GA, Hurrell JH, van Loon H (1998) A modulation of the mechanism of the semi-annual oscillation in the Southern Hemisphere. Tellus 50A:442–450

Mo KC, White GH (1985) Teleconnections in the Southern Hemisphere. Mon Wea Rev 113:22–37

Raphael MN (2004) A zonal wave 3 index for the Southern Hemisphere. Geophys Res Lett 31, doi:10.1029/2004GL020365

Schmidt GA et al (2005) Present-day atmospheric simulations using GISS ModelE: comparison to in situ, satellite and reanalysis data. J Clim (accepted for publication)

Simmonds I, Walland DJ (1998) Decadal and centennial variability of the southern semiannual oscillation simulated in the GFDL coupled GCM. Clim Dyn 14:45–53

Thompson DWJ, Solomon S (2002) Interpretation of recent Southern Hemisphere climate change. Science 296:895–899

Thompson DWJ, Wallace JM (2000) Annular modes in the extratropical circulation, I: month to month variability. J Clim 5:1000–1016

Trenberth KE (1980) Planetary waves at 500 mb in the Southern Hemisphere. Mon Wea Rev 108:1378–1389

Trenberth KE, Mo KC (1985) Blocking in the Southern Hemisphere. Mon Wea Rev 133:38–53

Trenberth KE, Large WG, Olson JG (1990) The mean annual cycle in global ocean wind stress. J Phys Oceanogr 20:1742–1760

Van Loon H (1991) A review of the surface climate of the Southern Hemisphere and some comparisons with the Northern Hemisphere. J Mar Syst 2:171–1994

Van Loon H, Jenne RL (1972) The zonal harmonic standing waves in the Southern Hemisphere. J Geophys Res 77:992–1003

Xu J-S, von Storch H, van Loon H (1990) The performance of four spectral GCMs in the Southern Hemisphere: the January and July climatology and the semiannual wave. J Clim 3:53–70